JOURNAL OF MATERIALS SCIENCE 32 (1997) 5191–5204

Toughening of polystyrene by natural rubber-based composite particles

Part III *Fracture mechanisms*

M. SCHNEIDER, T. PITH, M. LAMBLA*
Laboratoire d'Extrusion Réactive, Institut Charles Sadron (CRM-EAHP), 4, rue Boussingault, Strasbourg, France

Impact testing has allowed the toughness of PS blends to be correlated with the morphology of the dispersed rubber phase, which was a natural rubber (NR) in particle form, coated with a shell of polystyrene (PS) or polymethylmethacrylate (PMMA). PS subinclusions were also introduced into the NR core. The impact resistance of the prepared PS blends began to rise steeply at a particle content of about 18 wt%. Transmission electron microscopy (TEM) in combination with osmium tetroxide staining techniques, allowed direct analysis of the crazing and cavitation processes in the composite natural rubber particle-toughened PS blends. Bulk samples were studied at high and slow deformation speeds. Different deformation mechanisms were effective, depending on the location of the observed stress-whitened zone relative to the notch tip. The apparent fracture mechanisms in rubber-toughened PS blends were also studied by scanning electron microscopy. PS blends containing polydisperse natural rubber-based particles or monodisperse poly(*n*-butylacrylate)-based particles, and commercial high-impact polystyrene, were compared.

1. Introduction

Many investigations in the field of polymer toughening deal with high-impact polystyrene (HIPS) which is a classic example of a brittle thermoplastic polymer. They often focus on rubber content and the particle-size effect of the dispersed rubber phase on the toughness of PS [1–5, 32]. Another very important factor to be considered is the morphology of the rubber phase. Toughening particles must initiate a large number of crazes in PS and at the same time control craze breakdown in order to avoid premature fracture. For example, glass beads embedded in a PS matrix initiate a large number of crazes but do not reinforce PS to any degree [6]. This fact implies that controlled craze growth is very important. In this paper the fracture mechanisms of PS blends containing different composite natural rubber-based latex particles are presented. Emulsion polymerization processes allowed the microstructure of natural rubber-based latex particles to be varied [7]. A commercially available NR seed latex was coated with a shell of cross-linked polymethylmethacrylate or polystyrene. Rigid PS subinclusions were also introduced into the NR core in order to vary the mechanical properties of the rubber phase. All model blends were prepared in a co-rotating twin-screw extruder in order to ensure good reproducibility.

A novel continuous blend preparation method was applied for the incorporation of wet latexes directly into a co-rotating twin-screw extruder. The dispersion of the latex particles within the matrix could be improved and even tacky rubber particles, which do not yield free-flowing powders for the weight feeders of conventional polymer processing machines, could be incorporated into a PS matrix. The continuous blend preparation, the stress–strain properties and the fracture toughness of these materials were the subject of Parts I and II of this series [8, 9]. An important point of this work was electron microscopic observations of the failure mechanisms of PS blends containing NR-based latex particles with different morphologies. Failure processes in polymeric materials depend on numerous complex interacting phenomena which are not yet completely understood. The plastic deformation zone ahead of a sharp notch which served as stress concentrator, was analysed. This approach is often used for triaxial tension observations. Osmium staining techniques [10–14] allowed not only the rubber particle morphology to be observed, but made it possible to analyse crazing and cavitation processes in a partially broken notched Charpy specimen by transmission electron microscopy. In rubber-toughened PS, most of the impact energy is absorbed by the generation and growth of crazes in the matrix.

* Author to whom all correspondence should be addressed.

0022–2461

A number of publications [13, 15, 16] deal with the formation of crazes in PS, but they have some limitations because the crazing of cast thin films of PS by TEM was analysed at slow deformation speeds. Such techniques imply the absence of stress field interactions around dispersed rubber particles. In this paper, the toughening mechanism in a massive standard ASTM sample of the different PS blends was examined at high deformation speeds. Keskkula *et al.* [17] described a similar method for analysing the craze structure of stress-whitened high-impact polystyrene by transmission and scanning electron microscopy. High deformation speeds were particularly important, as most of the prepared PS blends which were reinforced by different composite natural rubber-based impact modifiers, could be deformed at slow strain rates up to 60% (ASTM-based tensile testing) but were not equally tough at high deformation speeds (ASTM-based impact testing). Furthermore, rubber particle damage at slow deformation speeds was studied in order to demonstrate the importance of rigid subinclusions on cavitation processes which are associated with crazing in standard ASTM-based tensile samples.

2. Experimental procedure

2.1. Materials

The PS matrix, Lacqrène 1240 ($M_n = 154\,700$; $M_w = 357\,600$; $M_z = 601\,700$; $T_g = 100\,^{\circ}C$) was kindly donated by Elf Atochem. A centrifuged, not cross-linked, NR latex (Revertex AR) supplied by Revertex Ltd, was used as a seed latex in a sequential emulsion polymerization. The detailed emulsion polymerization technique for the preparation of the composite natural rubber latexes and their TEM characterization have been described elsewhere [7]. All secondary polymers in the NR-based latex particles were cross-linked by 0.25 wt % ethylene glycol dimethacrylate (EGDMA). Furthermore, cross-linked (0.25 wt % EGDMA) poly(*n*-butylacrylate) (PBuA)-based composite latexes were synthesized semicontinously by ammonium persulphate initiation at 72 °C. Subinclusions were introduced by AIBN initiation analogous to the NR-based particles.

2.2. Mechanical tests

ASTM test samples were moulded on a Billon 150/150 injection-moulding machine at 210 °C and left at 23 °C and 50% relative humidity for 1 wk.

The Izod impact resistance of V-notched samples (based on ASTM D256) was obtained using a standardized Zwick pendulum impact testing machine. The bar dimensions were 63 mm × 12.8 mm × 6 mm. Tensile testing on dumb-bell samples (based on ASTM D638) was performed on a hydraulic Instron 8031 machine at room temperature. The elongation (strain rate 50 mm min^{-1}) was measured directly on the sample using extensometer.

2.3. Electron microscopy

A Philips EM 300 transmission electron microscope was used in order to observe ultramicrotome cuts of PS blends which were prepared in the following way. First a smooth surface of a PS blend was exposed to osmium tetroxide vapour for 48 h in order to stain the NR phase [10–14]. The staining not only enhanced the contrast for the microscopic viewing of the blend morphology but also hardened the rubber phase. In this way ultramicrotome cuts could be prepared without altering the particle morphology of the no longer soft natural rubber particles.

A Cambridge Instruments Stereoscan 120 scanning electron microscope was used for the examination of notched Izod fracture surfaces of the prepared PS blends which were coated by gold-vapour deposition before viewing. A Joel JSM 840 scanning electron microscope was used for the observation of the fracture surface of the commercial HIPS samples.

2.4. Investigation of toughening mechanisms

A standardized Zwick pendulum impact testing machine was used at 23 °C and 50% relative humidity in order to obtain partial crack propagation by adjusting the hammer weight for incomplete break of a V-notched ASTM D256-based specimen. In this way, it was possible to analyse the formation of crazes and the associated particle damage at a velocity of the striking nose at the moment of impact of approximately 3.0 m s^{-1}. A razor blade was introduced into the notch and lightly tapped on it. The partially cracked bar (still in one piece) was stained by osmium tetroxide vapour in order to fix the craze structure and harden the rubber particles prior to microtoming. Thin sections were cut with a diamond knife in a direction perpendicular to the fracture surface as indicated in Fig. 1. The arrows show how the sample was partially broken.

Furthermore, injection-moulded ASTM standard tensile samples were strained to break in a hydraulic Instron 8031 machine at room temperature. The strain rate was 50 mm min^{-1}. Sections were cut with an ultramicrotome perpendicular to the principal stress direction for TEM examination. Osmium tetroxide was used to stain and harden the rubber particles before microtoming.

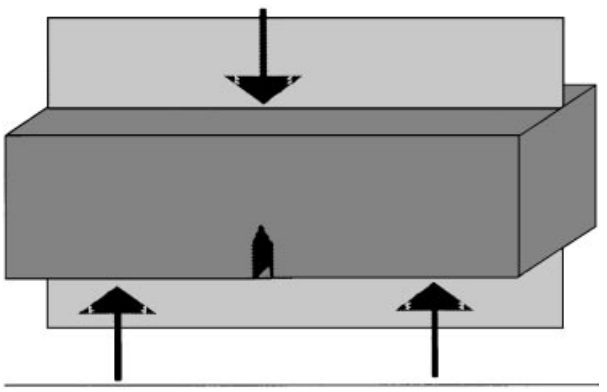

Figure 1 Plane of section for transmission electron microscopy.

3. Results and discussion

3.1. Effect of particle morphology and particle content

In order to study the effect of the particle morphology on the fracture toughness of the prepared PS blends, their standard ASTM notched Izod impact resistance was measured. The incorporated composite NR particles are represented schematically beside the corresponding graph of the impact energy in Fig. 2. The particle mass fraction had been systematically varied. A number of publications propose that polymer blends are only toughened when a critical inter-particle distance, τ_c, is attained. Wu [18, 19] reported that the ligament thickness or distance between two rubber particle surfaces, τ, is a characteristic property of the matrix polymer for a given mode, rate and temperature of deformation.

The number of prepared PS blends insufficient to determine precisely the brittle–ductile transition. However, curves a, c and d of Fig. 2 indicate that a critical concentration of about 18 wt % composite NR-based latex particles in the PS blends had to be exceeded before the impact resistance began to rise steeply. A plot of the impact resistance against the rubber content in the PS blends and not against the particle content as Fig. 2, indicates a common brittle to ductile transition at about 11% rubber for all reinforced PS blends. The toughness of the PS blends determines how much material can be deformed before individual craze breakdown leads to cracks and fracture of the blend. When the critical particle concentration is exceeded, no additional crazing is possible and the impact resistance cannot be improved further. The plateau obtained for high particle contents reflects this reasoning. PS blends containing less than 10 wt % toughening particles were brittle. The attained average inter-particle distance was large enough to provoke free craze growth until craze breakdown and premature fracture. More particles permit initiated crazes to be stopped at the next particle before reaching catastrophic craze lengths. The stress concentration factor at the particle equator can reach, at most, a factor of 2. When the inter-particle distance drops to smaller values, superposition of the particle stress fields occurs, leading to an even higher stress concentration between the particles. This effect causes a thickening of interconnecting crazes and more impact energy can be absorbed [20]. The determined critical particle concentration at about 18 wt % particles in the PS blends is in accordance with the literature [21] which reported a rubber volume content of more than 15% for effective rubber toughening of PS. This finding was explained by the superposition of the stress fields of neighbouring particles. Fig. 2 indicates that under testing conditions used, a common brittle–ductile transition occurred at the same critical particle mass fraction for different composite NR-based latex particles. In the case of the highly occluded particles (curve b) grafting of NR chains shifted τ_c to lower values. This effect was more pronounced when the rubber phase was purposely grafted by a higher reaction temperature or an initiation system which is known to graft NR during the preparation of the composite NR-based latex particles [9]. Many more rubber particles had to be incorporated in this case before the impact resistance began to rise.

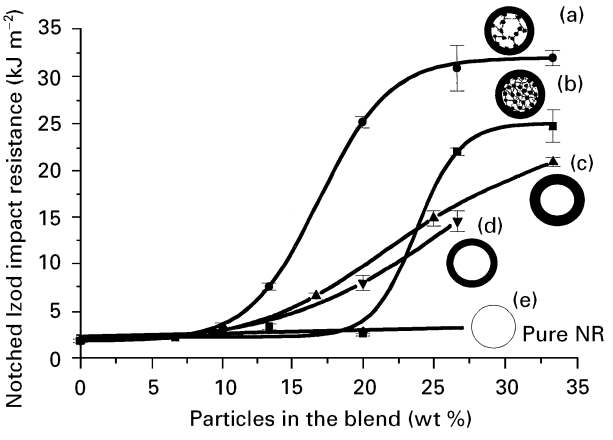

Figure 2 Comparison of the effectiveness of different natural-based composite latex particles as impact modifiers for PS. The core–shell particles (a, b, d) contain 25 wt % PMMA in the shell region, and particle (c) contains 40 wt % PMMA. 15 wt % and 30 wt % cross-linked PS subinclusions were introduced within the rubber core of the latex particles (a) and (b).

In Parts I and II of this series [8, 9], it was shown that PS-grafted NR particles were ineffective for the toughening of PS because of a high particle modulus. The used emulsion polymerization procedures determine the latex particle morphology and whether or not the NR chains are grafted. A core–shell arrangement of the polymer phases resulted when the bipolar redox initiation system tert.-butyl hydroperoxide/tetraethylene pentamine (tert.-BuHP/TEPA) in conjunction with a semicontinuous feeding process was used [7, 22, 23]. Polar polymethylmethacrylate was much more likely to produce the desired core–shell morphology than polystyrene. A large fraction of the styrene monomer formed many very small microdomains within the NR phase. The resulting modulus increase of PS-grafted NR particles in relation to PMMA-grafted rubber particles, impedes the craze preceding cavitation of the NR core. Fig. 3 shows the morphology of a PS blend with 25 wt % NR particles containing 40 wt % cross-linked PS in the shell region.

A large fraction of the styrene monomer polymerized in very small microdomains within the NR

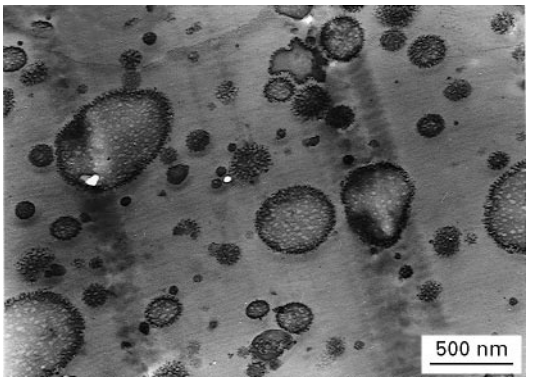

Figure 3 Transmission electron photomicrograph of a PS blend containing 25 wt % natural rubber particles with 40 wt % cross-linked PS in the shell region.

core. The diffuse interface of the PS-grafted NR particle and the PS matrix indicates an external PS-rich layer. Differences in the dispersion of NR particles coated with a shell of PS or PMMA were not noticed. However, changes in the shell composition can affect the interfacial adhesion which is due to physical interactions, such as surface free energy and molecular entanglement at the particle/PS matrix interface. Fig. 4 shows a scanning electron micrograph of the notched Izod fracture surface of a PS blend containing 25 wt % PS-grafted natural rubber particles. The PS-grafted rubber particles debonded from the PS matrix at impact and the toughness of the prepared PS blend could not be improved in relation to unmodified PS.

In the case of PS blends containing different PMMA-coated NR-based latex particles, cohesive failure of either the matrix or the incorporated NR particles took place and the PMMA-grafted NR particles with or without subinclusions did not debond [8, 9]. Replacing the cross-linked PMMA shell by cross-linked PS should have increased the adhesion between the incorporated latex particles and the PS matrix. However, Fig. 4 shows that the PS-coated NR particles debonded. In fact, Gent [24] established that the cavitation stress for polybutadiene and natural rubber-type rubbers depends linearly on the Young's modulus of the elastomer. On the other hand, the critical stress for debonding was found to decrease with increasing Young's modulus of the elastomer [24]. This anomaly was explained by a decrease of the interfacial adhesion caused by rheological effects. Impact testing and SEM of PS blends indicate that the degree of interfacial adhesion between the PS matrix and the incorporated composite NR-based latex particles was not a critical factor, because a PMMA shell, which is incompatible with the PS matrix, yielded very effective impact modifiers. The mechanical properties of the incorporated rubber phase, such as low modulus and rubber fibrillating rigid subinclusions, were crucial for the toughening of PS.

3.2. Fracture surfaces

In order to determine what role rubber particles play a toughening PS at fast deformation speeds, further SEM investigations of fracture surfaces were conducted. The SEM analysis of fracture surfaces, which was presented in Parts I and II [8, 9] always concerned the centre of notched Izod test sample. SEM investigations can also give insight into the dependence of the fracture mechanisms on the location of the observed failure zone relative to the notch tip. The centre of a notched Izod fracture surface of a PS blend reinforced by 13 wt % NR-based core–shell particles containing 15 wt % PS subinclusions in the core and 25 wt % PMMA in the shell, is shown in Fig. 5. The major failure mechanisms were crazing, fracture of rubber particles and particle debonding. The high magnification allows the occluded structure of the NR/cross-linked PS semi-interpenetrating network (semi-IPN) based core–shell particles, to be discerned. Fig. 6 shows a view of the Izod fracture surface at a distance of 100 μm from the notch tip.

Because the PS blend was submitted to high stresses at the notch root, the failure mechanisms changed. Virtually no debonded or cavitated particles could be found. It appears that the PS matrix had been more

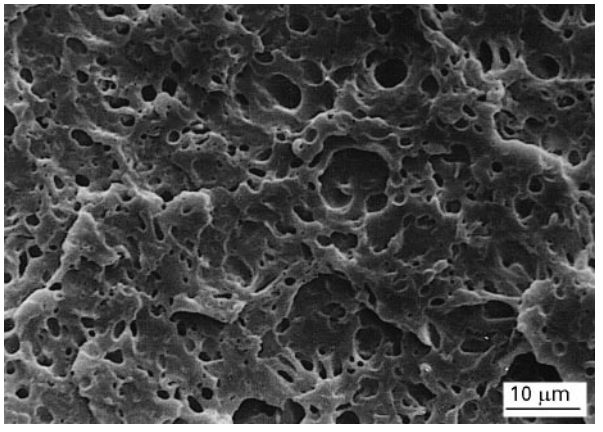

Figure 4 Scanning electron micrograph of the notched Izod fracture surface of a PS blend containing 25 wt % natural rubber particles with 40 wt % cross-linked PS in the shell region.

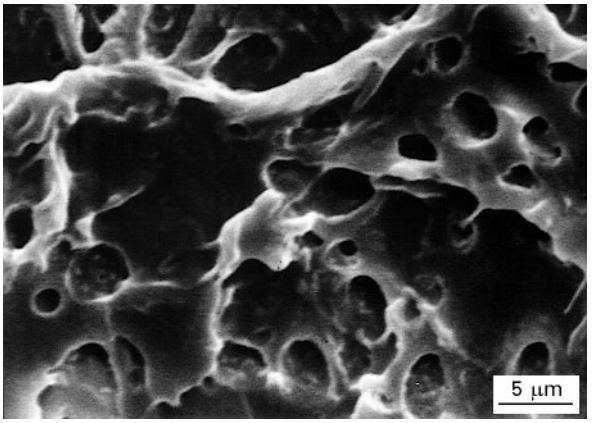

Figure 5 High magnification scanning electron micrograph of the notched Izod fracture surface of a PS blend reinforced by 13 wt % natural rubber particles containing 15 wt % cross-linked PS in the rubber core and 25 wt % cross-linked PMMA in the shell region. (Centre of the notched Izod test bar.)

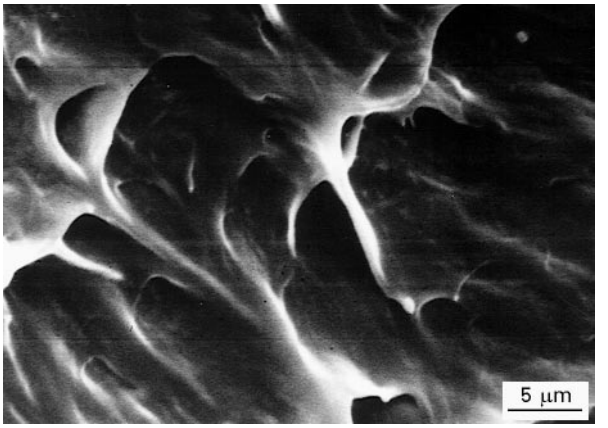

Figure 6 High-magnification scanning electron micrograph of the notched Izod fracture surface of a PS blend containing 13 wt % natural rubber particles with 15 wt % cross-linked PS in the rubber core and 25 wt % cross-linked PMMA in the shell region. (100 μm to the notch tip.)

extensively transformed into crazed matter. Similar observations were made when high-impact PS blends containing 27 wt % occluded core–shell particles were analysed by SEM. The morphology of the fracture surface near to the notch tip of PS blends containing NR-based core–shell particles without rigid PS occlusions, is shown in Fig. 7. The incorporated core–shell particles contained as much secondary polymer as the occluded core–shell particles, and the PS blends in Figs 7 and 8 contained the same NR mass fraction (10 wt %).

Figs 6 and 7 indicate intensified matrix deformation in relation to the centre of the fractured Izod bar. However, some of the core–shell particles debonded, because rigid subinclusions, which fibrillate the rubber phase at impact, were missing. The different deformation modes in the vicinity of the notch root and in the centre of the fracture surface could not be clearly detected at a low magnification, as shown in Fig. 8. However, SEM analysis of fractured PS blends containing excessively grafted NR-based core–shell particles or rubber particles without a shell, allowed to different degrees of matrix deformation near the notch tip and the centre of the Izod bar to be detected even at low magnification. Fig. 9 is a typical example of the fracture surface of a PS blend containing such ineffective toughening particles. Two distinct fracture zones can be distinguished. In a 1.5 mm large zone adjacent to the notch tip, the matrix has been extensively deformed followed by a surface which is characteristic for a brittle fracture. Increasing the content of the high-modulus NR particles to 27 wt % did not change the morphology of the fracture surface. The restricted size of the crazed zone explains why these PS blends could not be toughened. PS blends which contained only few toughening particles were not tough, either, because the stress fields of the rubber particles did not yet overlap. The morphology of the fracture surface of such blends reflects this finding; for example a PS blend containing only 7 wt % very effective occluded NR-based core–shell particles was not reinforced to any degree, as indicated in Fig. 2. Fig. 10 reveals a brittle fracture mode for the notch region as well as for the centre of such a broken Izod sample.

The high magnification view in Fig. 11 reveals fractured and debonded rubber particles. The PS matrix could not be transformed into crazed matter at such a low particle content and the fracture surface in the

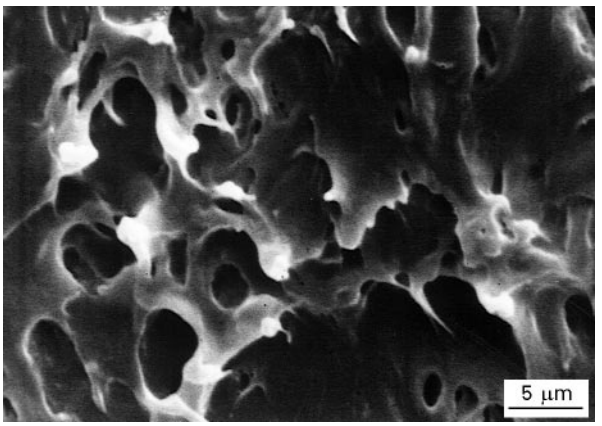

Figure 7 High-magnification scanning electron micrograph of the notched Izod fracture surface of a PS blend reinforced by 17 wt % natural rubber particles containing 40 wt % cross-linked PMMA in the shell region. (100 μm to the notch tip.)

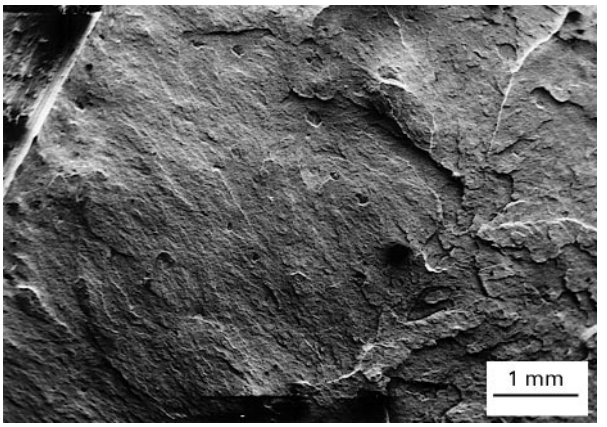

Figure 8 SEM overview of the notched Izod fracture surface of a PS blend reinforced by 13 wt % natural rubber particles containing 15 wt % cross-linked PS in the rubber core and 25 wt % cross-linked PMMA in the shell region.

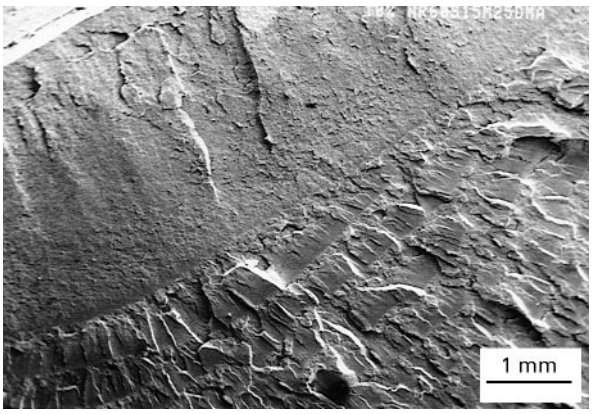

Figure 9 SEM view of the notched Izod fracture surface of a PS blend reinforced by 13 wt % grafted natural rubber particles containing 15 wt % cross-linked PS in the rubber core and 25 wt % cross-linked PMMA in the shell region.

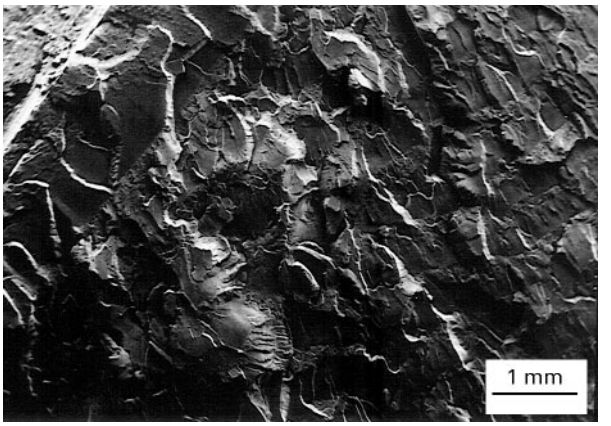

Figure 10 SEM overview of the notched Izod fracture surface of a PS blend containing 7 wt % NR particles with 30 wt % PS subinclusions and 25 wt % PMMA in the shell.

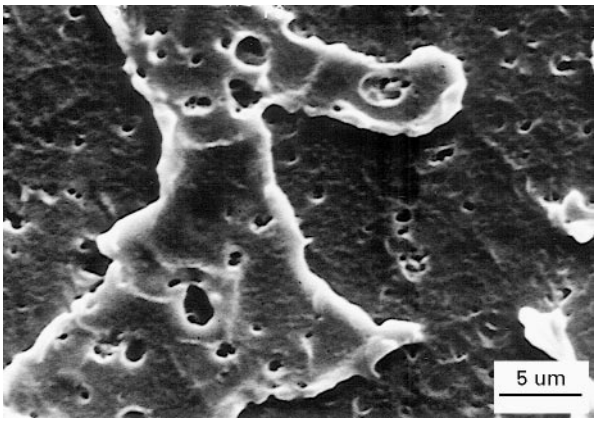

Figure 11 High-magnification scanning electron micrograph of the notched Izod fracture surface of a PS blend containing 7 wt % NR particles with 30 wt % PS subinclusions and 25 wt % PMMA in the shell. (Centre of the Izod test bar.)

centre of the notched Izod bar resembles the morphology of broken pure PS Izod test bars.

3.3. Toughening mechanisms in partially fractured bulk PS samples

The importance of PS inclusions within the NR-based core–shell particles on the fracture toughness of PS blends has been established in Part II of this series [9]. In order to understand the role of this type of rubber particle on the toughness of PS blends, the nucleation of crazes in these blends was analysed in detail by transmission electron microscopy. The sharp notch geometry used approximates the stress state at the tip of a propagating crack. An ultramicrotomed section of the notch tip of a partially broken Charpy test bar can be seen in Fig. 12, in which 27 wt % core–shell particles based on 60 wt % natural rubber/40 wt % cross-linked PS semi-IPNs had been incorporated. The transmission electron micrograph shows that the originally spherical composite NR particles were 200%–600% elongated in a zone immediately adjacent to the crack. This finding is somewhat surprising. Such high elongations of rubber particles imply that the PS matrix has been submitted to similar deformations. No crazes are visible. The high strain rates (impact conditions) at the notch root deformed the matrix polymer plastically. Owing to the stress concentration at the crack tip and the presence of the soft rubber particles, the toughening mechanism appears to have changed in the closest vicinity of the crack to a shear mechanism, as observed for some toughened grades of PMMA [2]. Fig. 13 shows a view of the propagated crack at a distance of 2 μm from the crack tip.

The transmission electronmicrographs of Figs 12 and 13 indicate that an important toughening mechanism in composite NR particle-toughened PS was crack deflection. Rigid subinclusions in the soft rubber phase multiplied the deviation of the crack path. By this means crack growth is limited below a critical rate and premature fracture can be avoided. It appears that the yielding mechanism of the PS matrix and the crack–deflection mechanism give rise to a synergistic

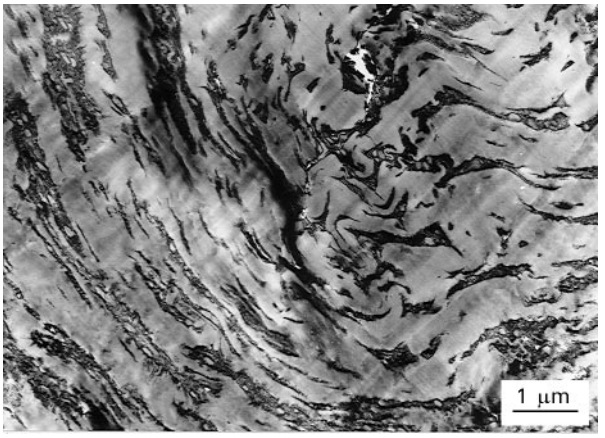

Figure 12 Transmission electron photomicrograph of a section of the crack tip region of a partially broken notched Charpy test bar of a PS blend toughened by NR-based core–shell particles containing 30 wt % PS subinclusions and 25 wt % PMMA in the shell region. (27 wt % particles in the blend.)

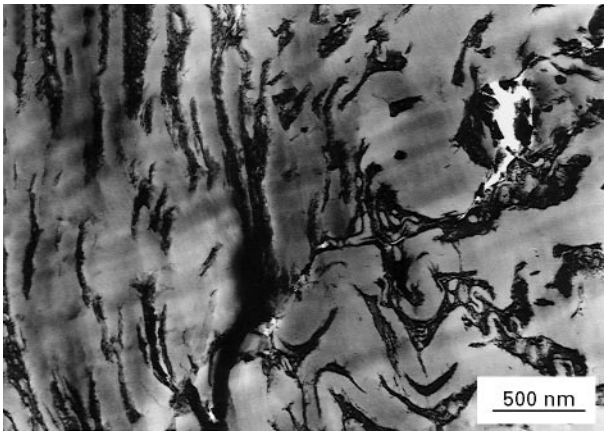

Figure 13 High-magnification TEM view of a section of the propagated crack in a partially broken notched Charpy test bar of a PS blend toughened by 27 wt % NR-based core–shell particles containing 30 wt % PS subinclusions within the rubber core and 25 wt % PMMA in the shell. (2 μm to the crack tip.)

toughening effect. Fig. 14 gives a detailed view of the yielded plastic zone 1 μm in front of the notch tip. The composite NR particles contained 45 wt % natural rubber which is much more in comparison with the "salami-like" polybutadiene-based particles in commercial HIPS.

The soft latex particles lowered the stress required for shear yielding at the notch tip before the stress for cavitation of rubber particles and subsequent crazing of the matrix polymer chains was achieved. Once the plastic yield zone was constituted, the resulting stress redistribution induced an increased stress when moving away from the notch root. Finite element analysis describes the stress redistribution when a plastic zone is present ahead of a notch tip [26]. Movement of the position of the stress maximum away from the notch tip has been treated for other notch geometries [27]. The high-magnification transmission electronmicrograph of Fig. 15 indicates that the matrix yielding mechanism was associated with cavitation processes in the elongated rubber particles when the damage

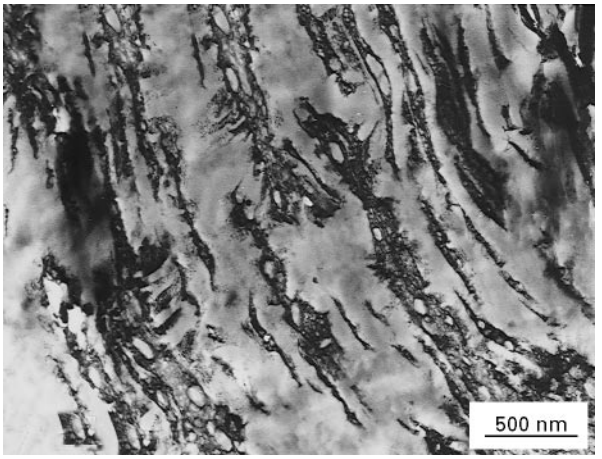

Figure 14 High-magnification TEM view of a section of the yielded zone of a partially broken notched Charpy test bar of a PS blend toughened by 27 wt % NR-based core–shell particles containing 30 wt % PS subinclusions within the rubber core and 25 wt % PMMA in the shell. (1 μm in front of the crack tip.)

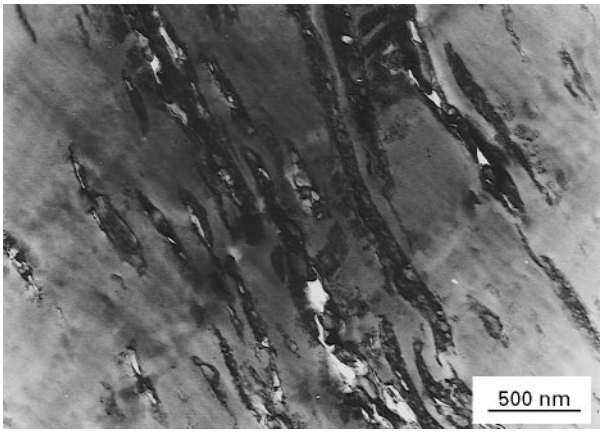

Figure 15 High-magnification TEM view of a section of the yielded zone at a distance of 5 μm to the propagated crack of a partially broken notched Charpy test bar of a PS blend toughened by 27 wt % NR-based core–shell particles containing 30 wt % PS subinclusions within the rubber core and 25 wt % PMMA in the shell region.

zone was analysed at a distance of about 5 μm to the propagated crack. In fact, the observed zone in Fig. 15 represents a transition region of a shear yielding mechanism in the immediate vicinity of the propagated crack to the very well-known crazing mechanism of PS. TEM investigations around the crack reveal that the composite NR particles were only slightly elongated when the crack plane was viewed further away from the damage zone. The matrix deformation mechanism had changed. Fig. 16 shows a profuse array of crazes at NR-based core–shell particles containing 40 wt % PS subinclusions. The stress concentration at a distance of about 30 μm laterally to crack tip region had been sufficient to initiate the classical crazing mechanism in PS. It can be seen how the occluded rubber particles behave at high deformation speeds in the bulk material near to the crack tip during Izod impact. A region with a profuse array of crazes and cavitated rubber particles was located in a zone which began approximately 30–40 μm laterally to advanced crack tip. Crazes with their length perpendicular to the loading direction grew predominately from the equatorial plane of micrometre-sized particles. Even when the particles were very close to each other, almost no crazes originated from the pole region of the particles. As the particles were strained in the direction of the tensile stress, the particles responded by internal rubber cavitation in order to compensate the dimensional changes imposed upon them. The importance of the PS inclusions within the rubber core can be deduced. They constrain the rubber phase which cavitated internally and no large voids were formed at the interface between the composite latex particle and the PS matrix. In Part I of this series [8] it was shown that pure NR latex particles debond from the matrix. Donald and Kramer [15, 16] established, by TEM studies of thin HIPS films, that unoccluded polybutadiene particles contract in a direction laterally to the stress field. The large voids which are formed contribute significantly to failure to crazes. Inferior mechanical properties of the PS blend result. Interpretation of the effect of the morphology of HIPS particles on the toughness of PS was complicated by the inhomogenity of the dispersed rubber phase, because small particles tended to be homogeneous and the larger particles contained subinclusions of the glassy matrix polymer. The use of tailor-made emulsion latexes in this study ensured that small, as well as large, particles contained rigid PS subinclusions which fibrillate the natural rubber core.

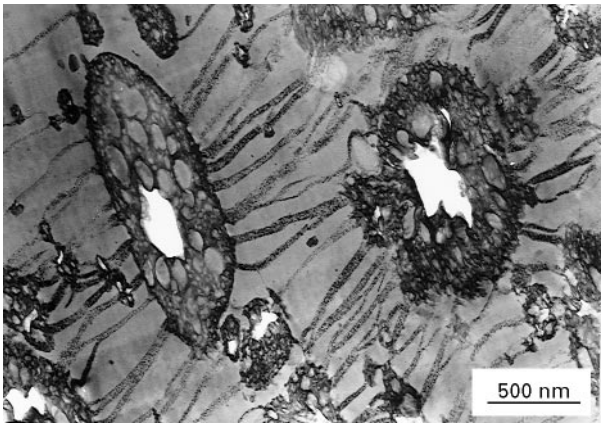

Figure 16 Transmission electron photomicrograph of a zone which is located 30 μm laterally to crack tip region of the notched Charpy test bar of a PS blend toughened by NR-based core–shell particles containing 30 wt % PS subinclusions within the rubber core and 25 wt % cross-linked PMMA in the shell. (27 wt % particles in the blend.)

It is known that particle size plays an important role in polymer toughening [1, 2]. Theoretical calculations show that the stress concentration at the particle surface is independent of the particle diameter and the size of the stress concentration zone corresponds to the particle radius. A minimum effective particle diameter of 40 nm for the toughening of PS was established, because the stress concentration zone must not be smaller than the minimum craze thickness

[21]. However, it is accepted that small particles (<1 μm) reinforce PS to a much lesser degree than large particles (2–5 μm) at a constant rubber content [17, 29]. The transmission electron micrograph in Fig. 16 reveals that both large micrometre-sized and small particles which are, in most cases, close to big particles, caused extensive crazing of the PS matrix. Large particles preferentially nucleated crazes, and small particles in the vicinity of big particles allowed the craze to grow in a bridge-like manner. These small encountered particles act as initiators for multiple new crazes which considerably increase the amount of the crazed matter. This finding is very important in order to understand the good mechanical properties of HIPS with a dual population of rubber particle sizes [29]. It should be noted, though, that isolated NR-based composite latex particles, which are smaller than 300 nm rarely nucleated crazes.

It appears that cavitation preferentially in large micrometre-sized but also in small-sized (< 400 nm) particles was the first step of the crazing mechanism in PS. From uncavitated particles, considerably fewer crazes originated. Several authors concluded that rubber particle size controls cavitation. They established that voids preferentially form in large-sized particles. These findings are in accordance with our results.

A model of Bucknall *et al.* [30, 31] is based on the principle that a particle cavitates when the strain energy released during cavitation is greater than the energy needed to form a cavity within the rubber particles. A similar model was developed by Dompas *et al.* [33, 34] and applied to poly(vinyl chloride)/methyl methacrylate–butadiene–styrene graft copolymer blends. Cavitation, in itself, cannot absorb much energy. However, Fig. 16 indicates that the created free surface in a NR-based latex particle provides a very effective craze nucleation site, which usually is situated close to a cavity within the natural rubber core. Fig. 17 gives a detailed view on the craze initiation site at a micrometre-sized composite NR-based particle in the neighbourhood of two smaller-sized rubber particles.The latex particles contain 40 wt % rigid PS subinclusions and 25% PMMA in the shell region. In addition to large-sized cavities (> 200 nm) within the rubber core, very small voids (< 50 nm) were found in the subsurface region of the rubber particle. These tiny voids were always located at the craze generation site on the surface of the incorporated rubber particles. The central cavity is formed prior to craze initiation at the periphery of the rubber particles. It is suggested that very small subsurface voids form in order to compensate the high local deformation at the particle surface where a craze originates. The localized subsurface voiding ensures that the rubber particle is not separated from the PS matrix. A decohesion would result in voids at the particle/matrix interface. These voids would grow and cause premature failure of the craze [15, 16].

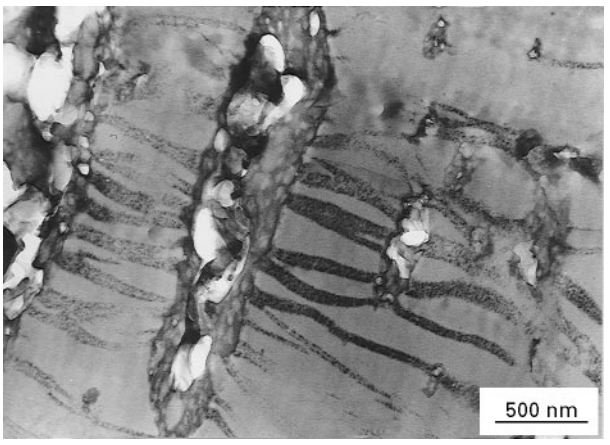

Figure 17 High-magnification TEM view of the craze initiation site at a micrometre-sized occluded NR-based core–shell particle in the neighbourhood of two smaller-sized rubber particles. (40 μm laterally to the propagated crack in a PS blend containing 27 wt % latex particles.)

Okamoto *et al.* [35] indicate that the improvement of bimodal HIPS is due to longer crazes initiated primarily at large rubber particles and not to an increased number of crazes compared to monomodal HIPS. Their model, which is based on a finite element method, suggests that crazes are first nucleated at large particles and then at small particles closest to a large particle, because the stress is highly concentrated there. On the other hand, models of Hobbs [36] and Wrotecki and de Charentenay [37] propose that crazes initiate from small rubber particles near to a large particle which stops the nucleated crazes. Our results indicate that primarily large cavitated rubber particles act as nucleation sites and terminators of crazes. The Okamoto model seems to describe well the crazing mechanism in PS blends toughened by composite NR-based particles which are very polydisperse in size.

The impact resistance of PS blends containing NR-based core–shell latex particles without rigid subinclusions was considerably smaller compared to polymer blends reinforced by occluded core–shell particles containing the same PMMA mass fraction in the shell or the same NR mass fraction in the latex particles [8]. A transmission electron micrograph of the damage zone around the crack root of a PS blend containing 33 wt % NR-based core–shell particles without rigid PS subinclusions is shown in Fig. 18. The PS blends which are compared in this section contain equivalent NR phase fractions; 20 wt % rubber phase (NR + PS subinclusions) had been incorporated.

Fig. 19 shows the propagated crack at a distance of 20 μm from the crack tip. The high-magnification view indicates that perfect core–shell particles had not been achieved during the emulsion polymerization [7]. Many very small-sized cross-linked PMMA microdomains can be distinguished.

The contours of the elongated rubber particles in Figs 18 and 19 clearly indicate the stress field in front of the crack tip and adjacent to the propagating crack. The incorporated composite latex particles contained 60% natural rubber instead of 45% in the case of core–shell particles with PS subinclusions. It can be seen that the softer rubber particles were elongated up to more than 500%. This finding indicates that the PS matrix underwent similar large-scale plastic deformations at the propagated crack. The deformation

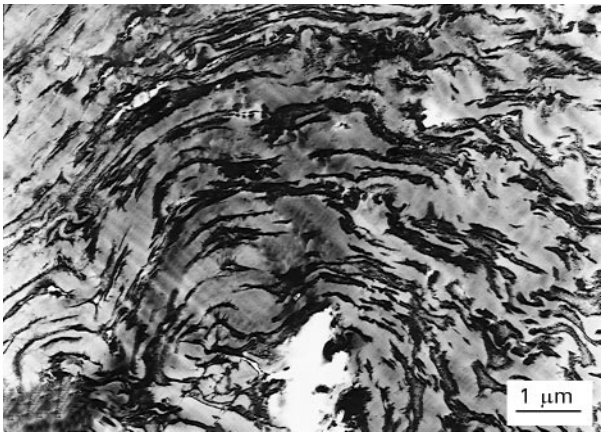

Figure 18 Transmission electron micrograph of a section of the crack-tip region of the notched Charpy test bar of a PS blend toughened by 33 wt % NR particles containing 40 wt % cross-linked PMMA in the shell region.

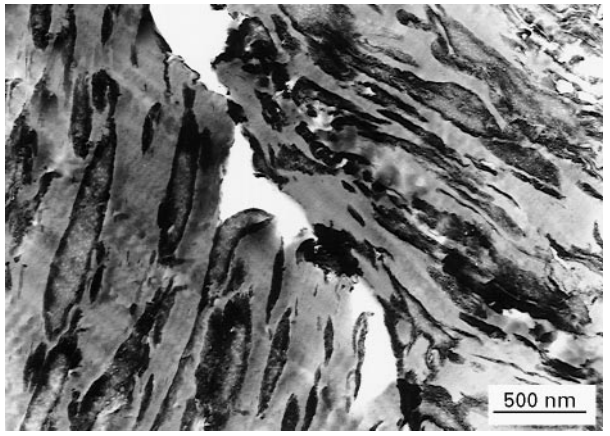

Figure 19 High-magnification TEM view of a section of the propagated crack of the notched Charpy test bar of a PS blend toughened by 33 wt % NR particles containing 40 wt % PMMA in the shell region. (20 μm to the crack tip.)

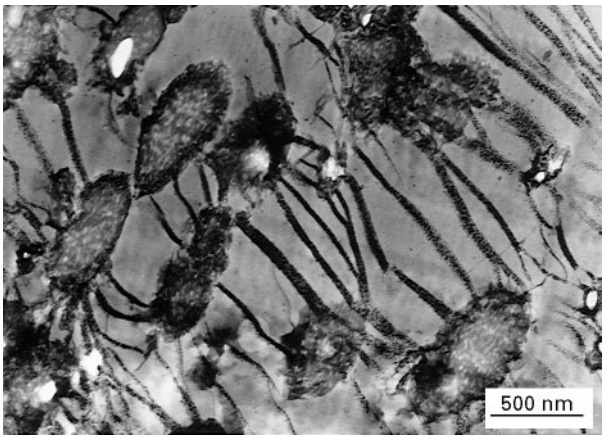

Figure 20 Transmission electron micrograph of a section which is located 30 μm laterally to crack tip region of the notched Charpy test bar of a PS blend toughened by 33 wt % NR-based latex particles containing 40 wt % cross-linked PMMA in the shell.

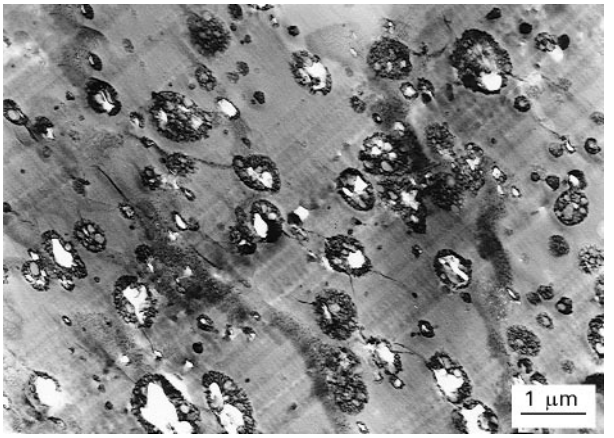

Figure 21 Transmission electron micrograph of the centre of a crazed standard ASTM tensile sample of a PS blend reinforced by 27 wt % natural rubber particles containing 30 wt % PS subinclusions within the rubber core and 25 wt % PMMA in the shell region.

mechanism of the PS matrix in the immediate vicinity of the crack tip did not change when core–shell particles without and with rigid PS subinclusions are compared. However, core–shell particles without rigid subinclusions did not promote crack deflection.

The failure mechanisms were also analysed further away from the propagated crack. Fig. 20 clearly shows that outside the yielded zone (30 μm laterally to the crack) the rubber particles were only slightly elongated and the matrix had been deformed by crazing, as already shown in Fig. 16 for a PS blend containing occluded core–shell particles. The major difference between Figs 16 and 20 is the craze preceding cavitation of the rubber core. Most of the NR particles without rigid PS subinclusions did not cavitate, as shown in Fig. 20. It is apparent that the toughening mechanism must have been dominated by rubber particle cavitation which could only be observed in the case of core–shell particles with rigid subinclusions. The particle morphology considerably affected the toughness of the prepared PS blends even though the matrix deformation mechanism by crazing did not change. The breadth of the crazes was not altered either. However, TEM suggests that the number of crazes was increased in the case of rubber particles containing rigid subinclusions. Hence, a higher impact resistance of the PS blend resulted. Fig. 21 shows that numerous cavities also developed within an NR particle containing PS subinclusions at slow deformation rates (50 mm min^{-1} instead of 3 m s^{-1}). TEM indicates that the PS subinclusion size had little effect on the failure mechanisms of the rubber particles. The incorporated rubber particles contained PS subinclusions which are very polydisperse in size. Some particles carry very large 200–400 nm sized occlusions, other particles only small-sized (< 50 nm) ones. All types of occluded particles had cavitated. This finding is consistent with impact data of PS blends reinforced with NR-based core–shell particles containing PS subinclusions of different sizes.

In Part II of this series [9] it was demonstrated that an increased mass fraction of PS within the NR phase increased the subinclusions size but had no effect on the fracture toughness of the prepared PS blends.

A large number of small occlusions was most effective. The impact resistance of PS blends containing the same mass fraction of simple NR-based core–shell particles without subinclusions was considerably decreased. Their mechanical properties could not be correlated with PS blends containing occluded core–shell particles. Furthermore, it was suggested that 10–30 nm sized subinclusions in the case of PS-grafted NR-based core–shell particles were ineffective because of an increased particle modulus. The PS subinclusions evenly distribute within the rubber phase and the average extent of the rubber zone between the PS occlusions was reduced to less than 15 nm. A batch emulsion polymerization increased the subinclusion size by a factor 6 when the same mass fraction of styrene monomer was polymerized within the NR seed latex [7]. TEM of fractured PS blends suggests that the rigid subinclusions within the NR phase must not be too small in order to leave a pure rubber zone with a minimum size in between. Theoretical models [30, 31, 33, 34] indicate a minimum particle size for rubber particle cavitation to occur. This concept is not restricted to whole rubber particles but can also be applied to composite rubber particles. It appears that a critical size of a pure natural rubber zone within the occluded core has to be exceeded before voiding can occur. This assumption gives another explanation why NR particles with a PS shell and many small-sized subinclusions were ineffective in reinforcing PS. Polymerizing more styrene within the NR seed latex increases the PS subinclusions size, but did not change the extent of the pure rubber zones within the core. The resulting impact resistance of PS blends containing such particles diminished, because natural rubber had been substituted by the increased mass fraction of PS in the particle. A linear dependence between the impact resistance and the NR weight fraction in PS blends containing different occluded NR based core–shell particles has been established in Part II of this series [9]. This result is consistent with the proposal that a minimal pure rubber zone within an occluded NR core is needed for cavitation to occur. Very large-sized subinclusions (e.g. 400 nm) cannot further change the toughening mechanism.

3.4. Particle damage at slow deformation speeds

Injection-moulded standard ASTM samples were craze-whitened to fracture in an hydraulic Instron machine at a deformation speed of 50 mm min^{-1}. Fig. 21 shows a typical micrograph of the ultramicrotome cut of such a crazed PS blend which was reinforced by 27 wt % NR particles containing 30 wt % cross-linked PS subinclusions within the rubber core and 25 wt % cross-linked PMMA in the shell region. The section was cut from the centre perpendicular to the deformation direction of the ASTM tensile specimen in order to observe rubber particle damage at slow deformation speeds. No attempt was made to keep the crazes in their extended state, as described by Keskkula *et al.* [17]. Prior to microtoming, the rubber phase was stained and hardened by osmium tetroxide vapour. Because the crazes were not fixed, as in the case of partially broken notched Izod test bars, only very few traces of crazes can be distinguished in Fig. 21. However, the craze preceding cavitation of the rubber phase is clearly visible. The tensile sample which contained 27 wt % composite NR particles had been strained to break. At slow deformation speeds (tensile testing) the matrix polymer chains could easily be transformed into crazed matter in order to attain elongations up to 60%. Theoretical models predict that the minimum particle diameter required for cavitation decreases drastically with the applied relative volume strain [31, 33]. Equation 1 relates the critical particle size for rubber cavitation, d_0, directly to the applied relative volume strain Δ [34]

$$d_0 = \frac{12(\gamma_r + \Gamma_{sc})}{K_r \Delta^{4/3}} \quad (1)$$

Γ_{sc} is the energy per unit area associated with chain scission, K_r is the rubber bulk modulus and γ_r is the van der Waals surface tension of the rubber. The relative volume strain is calculated as the $(1 - 2\nu_m)\varepsilon$ where ν_m is the Poisson's ratio of the glassy matrix and ε is the longitudinal strain. Large rubber particles will cavitate first and small rubber particles will cavitate in the later stages of the deformation process. For example, at a relative volume strain of 1%, a critical particle size of 200 nm is reached [34]. Hence, at the high volume strain of the studied PS blend, no critical minimal particle size for internal cavitation can be determined for the NR-based core–shell particles. In fact, composite natural rubber particles from less than 100 nm to 2 μm had cavitated. Similar observations can be made at fast deformation speeds in a partially fractured notched Izod test bar which is shown in Fig. 16. Internal rubber cavitation was always associated with crazes which originate from the surface of a rubber particle near to a cavity. These observations confirm that small-sized rubber particles are capable of contributing to the toughening of PS. In the preceding section it was established that the influence of the morphology of the dispersed rubber phase is very important at fast deformation speeds (impact testing). Fig. 22 gives a detailed view how occluded NR-based core–shell particles respond to an applied tensile stress at slow deformation speeds. Figs 21 and 22 show that not only one central cavity is formed, but several voids can be seen within occluded rubber particles. Thus, a separation of the rubber particle from the PS matrix which causes premature craze breakdown can be avoided. The introduced PS subinclusions constrained the soft rubber phase which failed, because rigid occlusions within the NR phase cannot be deformed, whereas the low-modulus rubber phase responded to the externally applied strain. In particular, hard occlusions which entrap a rubber zone in between, caused the rubber phase to cavitate in order to relieve the stress.

PS blends which contained 20 wt % pure NR particles could only be deformed to less than half the elongation at break of PS blends containing a comparable amount of rubber phase (NR + PS subinclusions) in core–shell particles with rigid PS

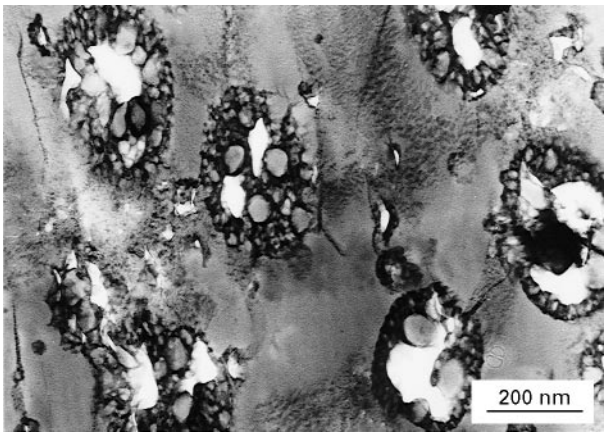

Figure 22 High-magnification TEM view of failure processes in natural rubber particles containing 30 wt % cross-linked PS subinclusions within the rubber core and 25 wt % cross-linked PMMA in the shell region. (Section of a crazed-whitened tensile sample of a PS blend containing 27 wt % composite particles.)

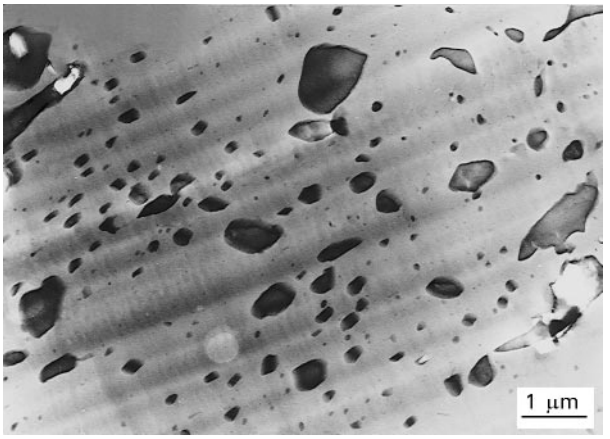

Figure 23 Transmission electron micrograph of the centre of a crazed standard ASTM tensile sample of a PS blend containing 20 wt % pure natural rubber particles.

subinclusions. At low deformation speeds, pure rubber particles were considerably less effective. They were completely ineffective at fast deformation speeds (impact testing), as indicated in Fig. 2.

Fig. 23 shows a transmission electron micrograph of a section of an ASTM dumb-bell sample which had been elongated to 28%, where it broke. Crazes cannot be distinguished because they had not been fixed. The fibril structure of the crazes might have been suppressed during the sample preparation or during the transmission electron microscopy. Virtually no cavitated particles can be seen. On the other hand, Figs 21 and 22 clearly show multiple cavities in the dispersed-composite NR particles. Rubber cavitation led to a reduction of constraint, allowing further matrix deformation to occur. This toughening mechanism was not effective in the case of PS blends containing pure rubber particles. Similar explanations have been put forward to explain the toughness of ABS [16] and toughened epoxy resins [38]. It should be noted, though, that the increase of toughness due to multiple crazing is much greater in magnitude. Fig. 2 indicates that the impact resistance of PS blends could not be improved by pure rubber particles. However, core–shell NR particles containing rigid PS subinclusions increased the impact energy of PS by a factor of more than 15. This result implies that the principal morphological feature controlling the deformation behaviour at fast and slow rates is certainly the particle morphology and not rubber particle size. Multiple cavitation of the rubber phase must precede the crazing process in tough PS blends.

A commercial impact modifier for polyvinyl chloride (KM 323B from Rohm and Haas) has also been tested as a possible toughening agent for PS. The particles are about 300 nm sized and have a core–shell morphology with a poly(*n*-butylacrylate) (PBuA)-based rubber core. Some PMMA microdomains are also embedded in the rubber core. The PMMA shell represents about 30% by volume and only 11% by radius of the latex particle. PS blends which were prepared by continuous extrusion, could not be toughened at a particle content of 10, 20 or 30 wt % of the commercial core–shell particles, due to a particle size which is too small for effective toughening of PS. A high cross-linking degree or an increased shear modulus of the PBuA rubber phase which shifts the craze preceding rubber cavitation to higher stresses [30, 31, 39] could be other possible causes for the low impact properties of the prepared blends. PS blends containing other small-sized polybutylacrylate-based core–shell particles are discussed in the following section. The elongation at break of all prepared PS blends containing PBuA-based latexes was found to be less than 5%. The deformation mechanisms in polymer blends containing such small particles were also studied. Even though small-sized latex particles did not toughen PS at fast or slow deformation speeds, they initiated crazes in a PS matrix, as shown in Fig. 24. The transmission electron micrograph contains a huge aggregate of latex particles which had been formed during the blend preparation process. Cavitation processes within the rubber particle agglomeration can be clearly distinguished. On the other hand, isolated rubber particles did not cavitate. This finding is consistent with the reasoning of the preceding paragraph. A latex particle aggregate can be represented as one large-sized rubber particle containing many small-sized rigid subinclusions. The occlusions in the latex agglomeration are formed by the rigid PMMA phase in the shell of the commercial latex particles. The latex particle aggregate shows multiple internal cavitation. This failure mechanism is comparable to occluded large-sized NR-based core–shell particles which cavitated at fast and slow deformation speeds.

Our results are consistent with real-time small-angle X-ray scattering studies by Bubeck *et al.* [40, 41] who concluded that non-crazing mechanisms occur before crazing in HIPS and ABS. Their data indicate that rubber particle cavitation and associated ligament bending of the surrounding matrix take place. Our TEM studies revealed internal cavitation in composite NR particles both at high and at slow deformation speeds. Dilatation measurements during the

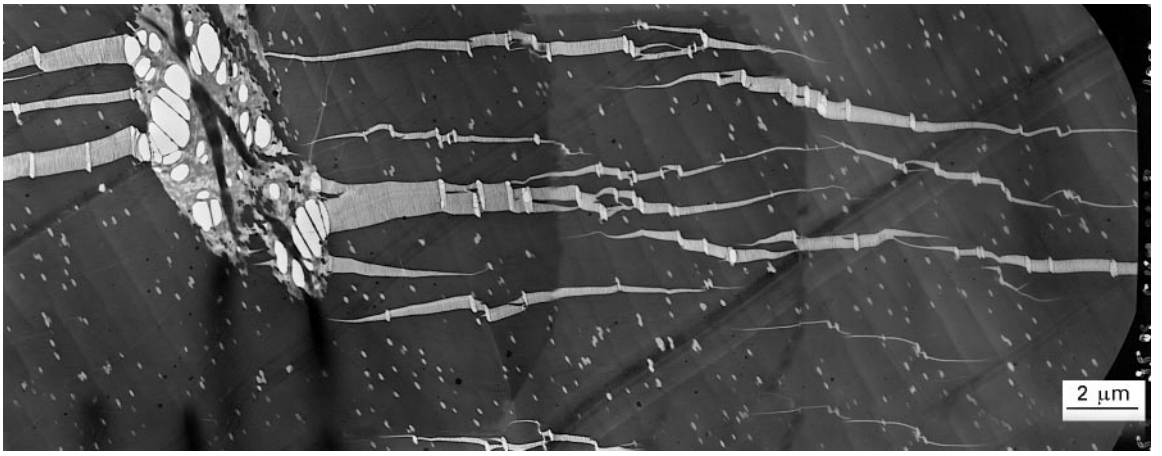

Figure 24 Transmission electron micrograph of crazes in the centre of a standard ASTM tensile sample of a PS blend containing 10 wt % KM 323B core–shell latex particles from Rohm and Haas.

deformation of rubber-toughened thermoplastics cannot precisely detect such non-crazing mechanisms [42–44].

3.5. Comparison of natural rubber, synthetic latex particles and HIPS

In Part I [8] we demonstrated that monodisperse 180 nm sized poly(*n*-butylacrylate) based core–shell particles proved to be too small for effective rubber toughening of a PS matrix. NR-based core–shell particles containing PS subinclusions could raise the impact resistance of the same matrix by a factor of more than 15 (supertough PS). In order to verify whether PS subinclusions could improve the performance of small and monodisperse PBuA-based toughening particles, 15 and 30 wt % cross-linked PS subinclusions were introduced into the rubber core, as in the case of the NR-based latex particles. However, PS blends containing 27 wt % small poly(*n*-butylacrylate)-based core–shell particles with rigid PS subinclusions were equally brittle and the impact resistance could not be improved. The prepared blends contained as much PBuA-based latex particles as the natural rubber-toughened PS blends. The *z*-average mean value of the size of the poly(*n*-butylacrylate) rubber core was 350 nm as obtained by photon correlation spectroscopy performed on a Malvern Autosizer II. Polydisperse natural rubber-based latex particles with a *z*-average mean size of 500 nm and monodisperse PBuA rubber-based particles are not directly comparable, because the poly(*n*-butylacrylate)-based latex did not contain large micrometre-sized particles. However, our results confirm data about PBuA-based core–shell particle-modified PS published by Cook *et al.* [45] who pointed out that submicrometre particles cannot reinforce PS. The brittle notched Izod fracture surface of a PS blend containing PBuA-based core–shell particles with 30 wt % cross-linked PS subinclusions and 25 wt % PMMA in the shell, is shown in Fig. 25. The mass fraction of the secondary polymers in PBuA-based composite latex particles and their morphology precisely corresponds to the NR-based core–shell particles used, containing PS subinclusions.

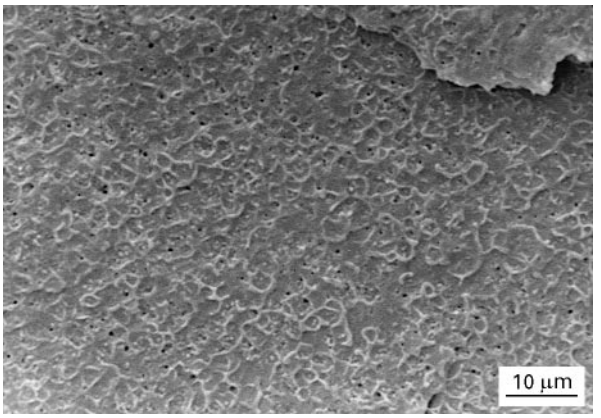

Figure 25 Scanning electron micrograph of the notched Izod fracture surface of a PS blend containing cross-linked poly(*n*-butylacrylate)-based core–shell particles with 30 wt % cross-linked PS subinclusions within the rubber core and 25 wt % cross-linked PMMA in the shell.

The achieved notched Izod impact resistance of composite NR particle-toughened PS blends (32.5 kJ m^{-2}) is about twice as high as the impact resistance of commercial HIPS produced by free-radical polymerization of styrene containing dissolved polybutadiene rubber. For example, the notched impact energy of a supertough HIPS sample of Elf Atochem (Lacqrene® 8350) was determined at only 14.0 kJ m^{-2}. The supertough HIPS contains an equivalent rubber mass fraction. It had been transformed and tested under the same conditions as the NR-toughened PS blends and could be directly compared: 13.0 kJ m^{-2} for the impact resistance, 55% elongation at break and 21 MPa for the yield stress, are given in the technical information note [46]. A view of the notched Izod fracture surface of the commercial HIPS is given in Fig. 26. The HIPS fracture surface exhibits clearly less crazed material than fracture surfaces of natural rubber-toughened PS blends. It can be seen that the incorporated rubber particles of the tested HIPS fracture at impact. The occluded structure of

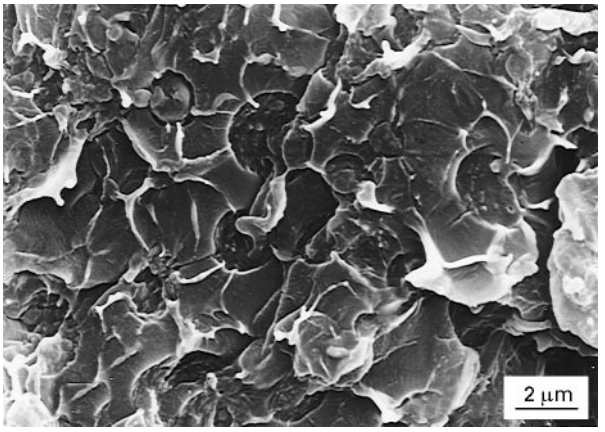

Figure 26 Scanning electron micrograph of the notched Izod fracture surface of a supertough HIPS (Lacqrene® 8350, Elf Atochem).

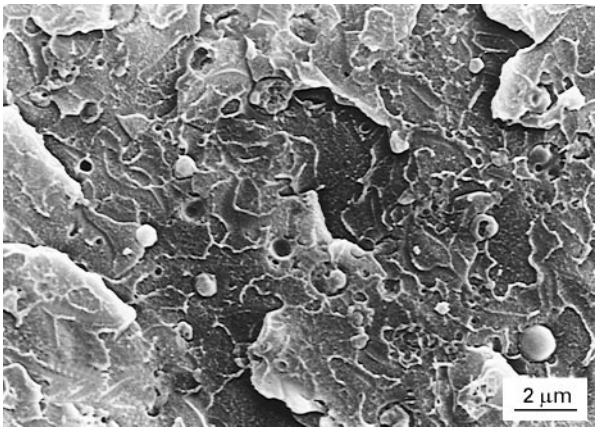

Figure 27 Scanning electron micrograph of the notched Izod fracture surface of a medium impact HIPS (Lacqrene® 2551, Elf Atochem).

classical HIPS particles can be distinguished. It appears that some of the polybutadiene-based rubber particles were separated from the PS matrix on impact. The very polydisperse particle-size distribution ranges from less than 1 μm to more than 8 μm. Very large-sized particles improve the crack resistance in relation to standard HIPS. Fig. 27 indicates that rubber particle/matrix separation is the predominant failure process in medium impact PS (Lacqrene® 2551, Elf Atochem). The measured notched Izod impact resistance of the medium-impact PS sample which contains three times less polybutadiene than the supertough HIPS, is 3.8 kJ m^{-2}; 4.0 kJ m^{-2} is given for the notched Izod impact resistance of the medium impact PS [47]. The occluded HIPS type particles of the medium-impact sample are clearly less polydisperse. Rubber particles in the range of less than 0.5–3 μm can be distinguished in the fracture surface of Fig. 27.

Similar failure observations in the fracture surface of broken HIPS samples were made by Keskulla *et al.* [17] and Schmitt [49]. On the other hand, NR-based core–shell particles containing PS subinclusions fibrillated extensively at impact and stayed well embedded in the matrix polymer. They cannot be distinguished in the Izod fracture surface. No rubber particle/matrix separation was detected in PS blends containing occluded NR-based core–shell particles. Very few of the simpler NR-based particles core–shell particles containing 40 or 25 wt % cross-linked PMMA in the shell region were separated from the matrix at impact. Nearly every pure NR particle debonded from the matrix, as indicated in Part I of this series [8]. The presented scanning electron micrographs of HIPS samples suggest that a rubber particle/PS matrix separation is an important failure mechanism to be considered in high-impact polystyrene.

A better adhesion of PS-coated particles to the matrix could not compensate the restricted toughening efficiency of high-modulus rubber particles. Furthermore, too many PS inclusions in the NR core were formed during the shell synthesis.

The superior performance of the different NR-based impact modifiers in relation to commercial HIPS can be further explained by the extremely high strain-hardening capacity of natural rubber which is unmatched by synthetic polymers. As the matrix is deformed, the rubber particles cavitate and are forced to stretch. When the rubber phase reaches extension ratios of 3 or more, the stress in the rubber becomes high enough to cause additional strain hardening. The excellent strain-hardening capacity of NR prevents premature failure of the PS blends.

4. Conclusions

Transmission electron microscopy proved to be a powerful tool to substantiate and elucidate failure mechanisms in toughened PS blends. Contrary to the conclusions of several previous dilation-based studies, electron microscopy revealed that rubber particle cavitation in combination with crazing occur in toughened PS blends. About 18 wt % composite natural rubber particles had to be incorporated into PS before the impact resistance was steeply increased, due to the superposition of the stress fields of neighbouring particles. Interfacial bonding between the impact modifier and the PS matrix was not required. All effective natural rubber-based composite latex particles were coated by a cross-linked PMMA shell.

The predominant deformation mechanisms in the bulk material of a partially fractured notched Izod bar at fast deformation speeds in crazing of the PS matrix and particle cavitation in occluded NR-based core–shell particles. Rubber cavitation is suppressed in craze-whitened PS blends containing simple core–shell particles. The PS matrix was plastically deformed in the immediate vicinity of the notch tip. No crazes or cavitated particles could be detected. The changed deformation mechanism is attributed to the stress concentration at the notch tip and the presence of soft, plastifying natural rubber particles. Subinclusions within composite NR-based latex particles multiply crack deflection, which is another important toughening mechanism of the prepared PS blends. There appears to be a direct relationship between the particle morphology and the toughening mechanism in the immediate vicinity of a propagated crack and

bulk PS material. Rubber particle/PS matrix separation is an important failure mechanism in commercial high-impact polystyrene. Occluded NR-based core–shell particles do not debond. Scanning electron microscopy revealed crazing, fracture of rubber particles and debonded rubber particles in the centre of fractured notched Izod bars. The PS matrix had been more intensively deformed into crazed matter in a zone near to the notch root.

Occluded natural rubber-based latex particles also failed by multiple rubber cavitation at slow deformation rates, because the PS subinclusions constrain the soft rubber phase. Pure rubber particles do not cavitate.

Rigid subinclusions did not improve the efficiency of small-sized poly(*n*-butylacrylate)-based core–shell particles to toughen PS. However, this approach to reinforce PS seems to be transferable to larger-sized industrial polybutadiene-based latex particles. The considerable increase of the toughness of PS containing occluded NR-based core–shell particles is attributed mainly to rubber cavitation. Rubber cavitation alone has little effect in absorbing energy. However, it initiates crazing, which is the main energy-absorbing mechanism in rubber-toughened PS blends.

Acknowledgements

The authors thank the European Economic Community for financing this research project (BRITE-EURAM Project BE - 4260). Valuable discussions of the results presented in this paper were held at the Deutsches Kunststoff-Institut (DKI) in Darmstadt, Germany and the Foundation for Research and Technology in Heraklion, Greece. The kind cooperation of Mr Morvan, Centre de Géochimie de la Surface, Strasbourg, for the transmission electron studies is gratefully acknowledged. Dr Hellmann, DKI, is thanked for providing the TEM Fig. 24

References

1. C. B. BUCKNALL, "Toughened Plastics" (Applied Science, London, 1977).
2. S. G. TURLEY and H. KESKKULA, *Polymer* **21** (1980) 466.
3. H. KESKULLA, "Rubber Toughened Plastics" (American Chemical Society, Washington, DC, 1989) p. 289.
4. E. PIORKOWSKA, A. S. ARGON and R. E. COHEN, *Macromolecules* **23** (1990) 3838.
5. G. DAGLI, A. S. ARGON and R. E. COHEN, *Polymer* **36** (1995) 2173.
6. R. E. LAVENGOOD, L. NICOLAIS and M. NARKIS, *J. Appl. Polym. Sci.* **17** (1973) 1173.
7. M. SCHNEIDER, T. PITH and M. LAMBLA, *J. Appl. Polym. Sci.*, **62** (1996) 273.
8. *Idem*, Toughening of Polystyrene by Natural Rubber Based Composite Particles: 1. Impact Reinforcement by PMMA and PS Grafted Core-Shell Particles. *J. Mater. Sci.* (in press).
9. *Idem*, Toughening of Polystyrene by Natural Rubber Based Composite Particles: 2. Influence of Internal Structure of PMMA Grafted Core-Shell Particles. *J. Mater. Sci.* (in press).
10. M. MATSUO, C. NOZAKI and Y. JYO, *Polym. Eng. Sci.* **9** (1969) 197.
11. K. KATO, *Polym. Lett.* **4** (1966) 35.
12. *Idem*, *J. Electron Micros.* **14** (1965) 220.
13. P. BEAHAN, A. THOMAS and M. BEVIS, *J. Mater. Sci.* **11** (1976) 1207.
14. K. KATO, *Koll-Z.Z. Polym.* **220** (1967) 24.
15. A. M. DONALD and E. J. KRAMER, *J. Appl. Polym. Sci.* **27** (1982) 3729.
16. *Idem*, *J. Mater. Sci.* **17** (1982) 2351.
17. H. KESKKULA, M. SCHWARZ and D. R. PAUL, *Polymer* **27** (1986) 211.
18. S. WU, *Polymer* **26** (1985) 1855.
19. *Idem*, *J. Appl. Polym. Sci.* **35** (1981) 549.
20. G. H. MICHLER, *Acta Polym.* **36** (1985) 285.
21. *Idem*, *Makromol. Chem. Macromol. Symp.* **38** (1990) 195.
22. R. J. CERESA, "Block and Graft Copolymerization" (Wiley-Interscience, London, 1973) Vol. 1, p. 47.
23. P. W. ALLEN, in "Chemistry and Physics of Rubberlike Substances" edited by L. Bateman (MacLaren, London, 1963) p. 97.
24. A. N. GENT, *J. Mater Sci.* **19** (1984) 1947.
25. O. FRANCK and J. LEHMANN, *Coll. Polym. Sci.* **264** (1986) 473.
26. J. R. GRIFFITHS and D. R. J. OWEN, *J. Mech. Phys. Solids* **19** (1971) 419.
27. R. TWICKLER, M. TWICKLER and W. DAHL, *Eng. Fract. Mech.* **24** (1986) 553.
28. S. G. TURLEY and H. KESKKULA, *Polymer* **21** (1980) 466.
29. BASF, US Pat. 4493 922.
30. A. LAZZERI and C. B. BUCKNALL, *J. Mater Sci.* **28** (1993) 6799.
31. C. B. BUCKNALL, A. KARPODINIS and X. C. ZHANG, *ibid.* **29** (1994) 3377.
32. N. C. LIU and W. E. BAKER, *Polym. Eng. Sci.* **32** (1992) 1695.
33. D. DOMPAS and G. GROENINCKX, *Polymer* **35** (1994) 4743.
34. D. DOMPAS, G. GROENINCKX, M. ISOGAWA, T. HASEGAWA and M. KADOKURA, *Polymer* **35** (1994) 4750.
35. Y. OKAMOTO, H. MIYAGI, M. KAKUGO and K. TAKAHASHI, *Macromolecules* **24** (1991) 5639.
36. S. Y. HOBBS, *Polym. Eng. Sci.* **26** (1986) 74.
37. C. WROTECKI and F. X. DE CHARENTENAY, *Deform. Yield. Fract. Polym.* **7** (1988) 51/1.
38. A. J. KINLOCH, S. J. SHAW, D. A. TOD and D. L. HUNSTON, *Polymer* **24** (1983) 1341.
39. A. LAZZERI and C. B. BUCKNALL, *Polymer* **36** (1995) 2895.
40. R. A. BUBECK, D. J. BUCKLEY, E. J. KRAMER and H. R. BROWN, *J. Mater Sci.* **26** (1991) 6249.
41. R. A. BUBECK, J. A. BLAZY, E. J. KRAMER, D. J. BUCKLEY and H. R. BROWN, *Mater. Res. Soc. Symp. Proc.* **79** (1987) 293.
42. C. B. BUCKNALL and D. CLAYTON, *J. Mater Sci.* **7** (1972) 202.
43. C. B. BUCKNALL and C. J. PAGE, *ibid.* **17** (1982) 808.
44. C. B. BUCKNALL, P. DAVIES and I. K. PARTRIDGE, *ibid.* **22** (1987) 1341.
45. D. G. COOK, A. RUDIN and A. PLUMTREE, *J. Appl. Polym. Sci.* **48** (1993) 75.
46. Lacqrene 8350, Technical Information Note, Elf Atochem, France, March, 1995.
47. Lacqrene 2551, Technical Information Note, Elf Atochem, France, February, 1995.
48. J. A. SCHMITT, *J. Appl. Polym. Sci.* **12** (1968) 533.

Received 3 January 1996
and accepted 4 April 1997